Supported Pt Nanoclusters on Single-Layer MoS2 for the Detection of Cortisol: From Atomistic Scale to Device Modeling

Gabriele Boschetto, Stefania Carapezzi, Aida Todri-Sanial

Supported Pt Nanoclusters on Single-Layer MoS_2 for the Detection of Cortisol: From Atomistic Scale to Device Modeling

Gabriele Boschetto[1], Stefania Carapezzi[1], Aida Todri-Sanial[1,2]

[1]*Laboratory of Computer Science, Robotics, and Microelectronics, University of Montpellier, CNRS, 161 Rue Ada, 34095 Montpellier, France*

[2]*Department of Electrical Engineering, Eindhoven University of Technology, Groene Loper 3, 5612 AE Eindhoven, Netherlands*

Email: gabriele.boschetto@lirmm.fr; aida.todri@lirmm.fr

Abstract

The development of non-enzymatic sensors is a challenge which requires, on the one hand, careful design of the sensing materials with respect to the chosen analyte, and on the other hand, suitable device architectures. In this work, we propose single-layer molybdenum disulfide (MoS_2) decorated with sub-nanometer Pt clusters as the sensing platform for the detection of cortisol. The aim is to assess the suitability of such a sensing platform for the development of wearable and portable cortisol sensors. For this study, we performed multi-scale computer simulations at the materials level up to device scale. First, ab initio simulations within the framework of density functional theory (DFT) allowed us to gain insights into the interaction, at the atomic level, between the analyte (cortisol) and the sensing platform (MoS_2/Pt). Then, by carrying out technology computer-aided design (TCAD) simulations, we were able to consider a device architecture and investigate its performance as cortisol sensor. Following our multi-scale simulation strategy, we were able to assess the proposed field-effect transistor (FET) sensor, whose channel is made of Pt-decorated MoS_2. The sensing mechanism relies on the chemiresistive response of the device to the adsorption of cortisol on the channel, which leads to a charge transfer from the analyte to the substrate and, consequently, to the measurable shift in the gate voltage threshold of the FET. Our findings suggest that both the choice of the sensing materials and the proposed FET architecture are suitable for detecting cortisol by non-enzymatic means, as we predict a maximum theoretical gate voltage shift of 780 mV in ideal conditions. We may expect our results to provide the necessary basis to develop highly sensitive non-enzymatic cortisol sensors based on 2D materials decorated with Pt nanoclusters.

1 Introduction

The design and development of wearable and portable biosensors have revolutionized modern healthcare. Smart watches,[1,2] contact lenses,[3,4] skin patches and tattoos,[5,6] all with the capability of measuring specific biomarkers in the human body, are the outstanding result of the interplay between the discovery of novel materials and improved device architectures.[7] Furthermore, the ubiquitous online connectivity has also enabled the collection and post-processing of medical data both remotely and at the patient's level. This is known as the Internet of Medical Things (IoMT).[8]

In this context, non-invasive wearable sensors allow the continuous (self-)monitoring of the patients' health status, which plays a pivotal role in desease prevention. For instance, it is widely known that pre-syntomatic screening and early detection can greatly reduce the risk of cardiovascular diseases (CVDs),[9,10] the leading cause of mortality in the world.[11,12] Importantly, the insurgence of CVDs is often correlated with variation in blood pressure and raised levels of glucose and lipids in the blood,[13,14] which could all be measured. One biomarker of particular interest is cortisol, a steroid hormone often associated with increased stress, which also appears to have a correlation with CVDs and, more generally, with a compromised immune state.[15,16] There exists a host of detection techniques dedicated to cortisol sensing, such as surface plasmon resonance,[17] chromatographic and optical sensing based on immunoassays,[18] and electrochemical sensors.[19] Mainly, such techniques involve the use of sophisticated equipment, available only in diagnostic laboratories. Although these provide high-sensitivity, they are expensive and experienced users are necessary to carry out the measurements, which generally require long time. Thus, these techniques are not suitable for point-of-care (POC) applications, and there is the need to develop simple and cheap POC miniaturized devices, with undemanding sample preparation and assaying. It is then no surprise that in recent years considerable effort has been devoted to the development of non-invasive wearable and portable cortisol sensors.[20–25] In this regard, chemiresistive sensors could very well provide a valid solution.[26–28] The sensing principle of such devices is the change of conductivity of the device channel, due to the surface adsorption of the chosen analyte.

To develop highly sensitive chemiresistive sensors, the proper choice of the sensing material, which will constitute the device channel, is crucial. For instance, two-dimensional (2D) materials have recently attracted significant interest for their desirable me-

chanical, electrical, and optical properties, and because of their inherent reduced dimensionality,[29,30] which allows the fabrication of very compact and flexible devices. Among 2D materials, single-layer molybdenum disulfide (MoS_2) has been widely explored for the fabrication of field-effect transistor (FET) sensors due to its direct band gap of ∼1.8 eV, good carrier mobility, and chemical stability.[31–34] However, the bare material is usually not suitable to be used in a sensing device, as it lacks chemical selectivity. To overcome such a limitation, common strategies include surface functionalization with antibodies and/or enzymes (enzymatic sensing),[35–37] and surface engineering via doping, decoration with metal nanoparticles, and purposeful generation of defects (non-enzymatic sensing).[38–40] The latter approach offers several advantages, such as easier fabrication, higher stability, faster response, and the possibility to finely tune the properties of the sensing platform. On the other hand, the mechanism of interaction between the analyte and the sensing platform is not always clear, even more with a relatively large molecule as cortisol (if compared to smaller common biomarkers like glucose and dopamine). Thus, understanding the analyte/substrate interaction is the first necessary step for the design and fabrication of high performing sensing devices.

In this work, we investigate by means of multi-scale computer simulations single-layer MoS_2 decorated with sub-nanometer Pt nanoparticles as the sensing platform for cortisol, to assess the feasibility of such a non-enzymatic sensing approach. First, we carry out density functional theory (DFT) simulations to thoroughly predict and assess the interaction, at the atomic level, between supported Pt nanoclusters of increasing size and the target analyte. Then, as a proof of concept we use the results obtained with DFT to simulate by technology computer-assisted design (TCAD) a MoS_2 FET as the chemiresistive sensor for cortisol detection. We do so to probe the chemiresistive effect upon cortisol adsorption on the device channel. To the best of our knowledge, this is the first time such a multi-scale simulation approach has been employed to investigate MoS_2 chemiresistors for the detection of cortisol. On the one hand, first-principles simulations with DFT have been proven extremely useful to study the analyte/substrate interaction.[41–45] On the other hand, device simulations are an invaluable tool to grasp device operation and to assist for its optimization. In this regard, industry-level TCAD technique is particularly attractive for its robustness, possibility to perform multi-physics simulations, and efficiency in terms of computational time. TCAD tools are commercial software suites which allow to apply finite elements analysis calculations to solve the partial differential equations describing device physics. TCAD is suitable to simulate electrical transport of devices in diffusive regime, that is when drift-diffusion (DD) equations apply.[46] This is mostly the case in sensor devices.[47,48]

This paper is organized as follows: the following section (Simulation Details) will focus on describing the setup of our multi-scale DFT-TCAD simulations, together with the models employed. In Results and Discussion, we present and discuss our simulation results on decorated MoS_2, its interaction with cortisol, and the device response. The final section contains the Conclusions.

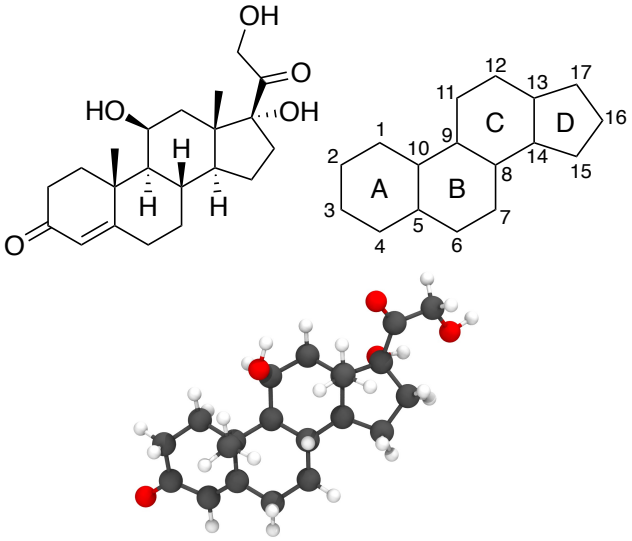

Figure 1: Chemical structure of cortisol, together with its C atom numbering and ring labelling. Its optimized structure at the DFT level is also shown.

2 Simulation Details

2.1 Materials Modeling with DFT

In this work, we explored the interaction between cortisol and sub-nanometer Pt nanoclusters (NCs) supported on single-layer MoS_2. The structures of the NCs were taken from the work of Shi and co-authors,[49] who carried out a combined experimental and theoretical study to accurately determine the atomic structure of supported Pt NCs on MoS_2. Here, we considered Pt_n clusters of increasing size, with n = 9, 13, 16, 20. Then, we placed cortisol above each of the four NCs, focusing on the reactivity of its carbonyl group attached to the ring A (see Figure 1). We chose this group as its good reactivity was already reported in the literature,[50–52] and our previous studies[53] also corroborated this. As our simulations were carried out in periodic boundary conditions, we ensured that the simulation cells were large enough to avoid any spurious interaction of cortisol with its periodic images: thus, we constructed an orthorombic $8\times4\times1$ MoS_2 supercell with at least 15 Å of vacuum padding in the out-of-plane direction. Such a simulation cell corresponds to a surface area of $\sim5.5\times10^{-14}$ cm^2 and a nanoparticle density of roughly 1.8 cm^{-2}, in line with the experimental findings of Shi et al.[49] For each NC, we tested different adsorption sites, as shown in Figure 2: two vertices (A and C), one edge site (B), and one site at the centre of the largest NC (D). Then, the structures were fully relaxed with no constraints, and their stability was assessed by computing the adsorption energy (E_{ads}). We defined this quantity as:

$$E_{ads} = E_{a+b} - (E_a + E_b) \quad (1)$$

where E_{a+b} is the total energy of the MoS_2/Pt_n/cortisol system, whereas E_a and E_b are the total energies of the isolated fragments (that is, cortisol and MoS_2/Pt_n). As we used localized orbitals (details of which will be given shortly), we took into account the

basis set superposition error (BSSE) by including the counterpoise correction[54] in our total energy calculations.

Computer simulations were carried out at the DFT level by using QuantumATK T-2022.03[55,56] atomic-scale modelling software. We carried out all simulations in vacuum using the Perdew-Burke-Ernzerhof (PBE) exchange-correlation functional,[57] and we modelled core electrons by using norm-conserving pseudopotentials from the PseudoDojo library.[58] We used localized orbitals within the LCAO (Linear Combination of Atomic Orbitals) formalism with a density-mesh cut-off of 200 Ry, and we used the QuantumATK-optimized Medium basis set for geometry optimizations. The High basis set was used for single-point and properties calculations. To take into account dispersion effects, we employed the D2 correction by Grimme.[59] A **k**-point mesh defined by a $2 \times 2 \times 1$ Monkhorst-Pack (MP) grid[60] was used throughout our simulations, whereas for computing the density of states (DOS) we chose a $4 \times 4 \times 1$ MP grid. All geometry optimizations were converged with residual atomic forces no larger than 0.03 eV/Å. To compute net atomic charges, we chose to employ the electron density partitioning scheme of the DDEC6 method with the CHARGEMOL program.[61] The DDEC6 method has the advantage to provide chemically meaningful charges that are independent of the basis set type and size, as opposed to the widely used Mulliken population analysis.[62,63]

As we were interested in assessing a non-enzymatic sensing platform, and as in our simulations we assumed the direct contact between cortisol and the supported Pt nanoclusters, we proposed a back-gated MoS_2 FET as a proof-of-concept device (see Figure 3). Results obtained with DFT in terms of charge transfer were used as the input for the following TCAD device simulations. The total charge on the MoS_2 channel before and after the adsorption of cortisol was the key quantity to assess the device chemiresistive response.

2.2 Device Modeling with TCAD

We used Synopsys Sentaurus Device[64] as drift-diffusion (DD) simulation engine. The geometry of our simulated MoS_2 FET sensor is shown in Figure 3. The monolayer MoS_2 (thickness 0.6 nm) sits on top of a SiO_2 substrate (thickness 10 nm). The MoS_2 channel is 1-μm long. Source and drain contacts are on top of the MoS_2/Pt_n channel, whereas a back-gate contact is located at the bottom of the oxide layer. The size of the channel ensures that a large number of scattering centers are present therein, and we can assume that the electrical conduction is correctly described by scattering-dominated DD charge transport.[65,66]

The following DFT-calculated material parameters for monolayer MoS_2 have been used as input for our TCAD simulations: band gap $E_g = 1.78$ eV, electron affinity $\chi = 3.9$ eV, effective relative permittivity $\varepsilon_r = 3.54$, electron effective mass $m_e = 0.51\ m_0$ and hole effective mass $m_h = 0.59\ m_0$, with m_0 being the free electron mass. The SDevice Multivalley 2D density-of-states (DOS) model has been used (option `dospower` = 1) to account for the impact of strong geometric confinement over energy dependence of DOS in monolayer MoS_2. For the sake of simplicity, the contacts have been considered Ohmic and no contact resistance has been included. We point out that this has been achieved

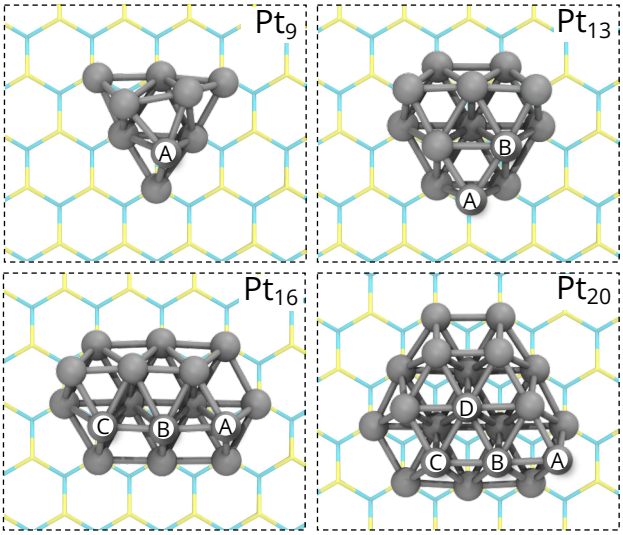

Figure 2: Optimized structures of the four Pt_n NCs (n = 9, 13, 16, 20) supported on MoS_2 considered in this study. Geometry optimizations were carried out at the PBE-D2 level. For each cluster, the tested adsorption sites for the adsorption of cortisol are also marked: two vertex sites (A and C), one edge site (B), and one site at the centre of the largest cluster (D).

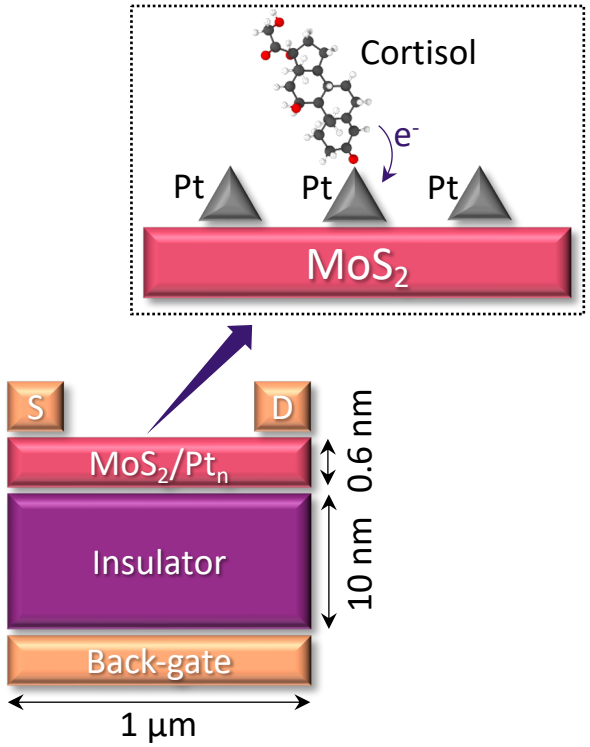

Figure 3: Schematics of the 2D simulated MoS_2 back-gate FET sensor device (not to scale). An uniform n-doping of the MoS_2 channel is considered to take into account the effect of charge transfer from the Pt clusters to MoS_2. Similarly, the additional cortisol-to-MoS_2 charge transfer is treated as a corresponding increased value of the doping density.

with semi-metal Bi contacts on MoS_2, as experimentally demonstrated in a recent work.[67] Finally, we have assumed the electron mobility to have the constant value of 200 $cm^2/(V \cdot s)$, which is in the range of experimental and theoretically calculated values of MoS_2 mobilities.[68,69]

We have simulated with TCAD the net charge on decorated MoS_2, with and without the presence of cortisol, as equivalent to the variation of n-doping. This allowed us to simulate the response of the device before and after the adsorption of cortisol. A similar approach has been already used to mimic the effect of NO_2 gas adsorption on carbon nanotube FET.[47,48] However, in that case the doping was extracted *ex-post* by calibrating the TCAD simulations with experimental data, whereas in the present case we have constructed a multi-scale modeling approach. The n-doping was obtained from the DFT-computed net charge on decorated MoS_2 with and without the presence of cortisol. The conversion of DDEC charges into equivalent n-doping (N) was made via the following equation:

$$N = \frac{\Delta Q_{MoS_2}}{A \cdot h} , \quad (2)$$

where ΔQ_{MoS_2} is the net charge on MoS_2 before (after) the adsorption of cortisol, A is the surface area of MoS_2 given by the DFT simulation cell (5.5×10^{-14} cm^2, as mentioned above), and h is the thickess of MoS_2, here taken as 0.6 nm.

3 Results and Discussion

The aim of this work is to investigate supported Pt nanoclusters of increasing size on single-layer MoS_2 for the non-enzymatic detection of cortisol. To do so, we first focus on the sensing material, that is Pt-decorated MoS_2. By carrying out DFT simulations, we elucidate how the presence of Pt nanoclusters affects the electronic properties of the material. Then, we look at the adsorption mechanism of cortisol on decorated MoS_2, and we predict the material's response to the presence of the analyte by computing the amount of charge transfer. Finally, to test our proposed sensing strategy involving the chemiresistive mechanism, we use the DFT-computed charges to carry our TCAD device simulations on MoS_2 FET sensors.

3.1 Properties of MoS_2 Decorated with Pt Nanoclusters

In this section, we focus on the structural, electronic, and charge-transfer properties of metal-decorated MoS_2. Our aim is to understand how decorating the material with small Pt clusters may affect its properties. This part of the work allows us to assess the suitability of the chosen sensing platform, that is, single-layer MoS_2 decorated with sub-nanometer Pt NCs of increasing size: Pt_9, Pt_{13}, Pt_{16}, and Pt_{20}. As already mentioned, the structure of each NC was validated both experimentally and theoretically.[49]

Following full relaxation of the atomic coordinates, we found no significant distortion of the MoS_2 structure upon decoration with Pt NCs, with the only exception of a limited out-of-plane bending in the proximity of the contact area. We found the average separation distance between MoS_2 and Pt NCs to range between 2.05 and 2.16 Å, suggesting a rather strong MoS_2/Pt_n interaction. To corroborate this, we computed the adsorption energy (E_{ads}) of each NC on MoS_2, and to make results comparable among clusters of different size we scaled E_{ads} per contact Pt atom. In addition, we decomposed such a quantity into its dispersion and electrostatic contributions. Our results suggest that, on average, E_{ads} decreases with the increase of the number of Pt atoms in contact with the MoS_2 support: we found -1.47 eV/atom, -1.60 eV/atom, -1.41 eV/atom, and -1.37 eV/atom for Pt_9, Pt_{13}, Pt_{16}, and Pt_{20}, respectively. In addition, we could also observe that dispersion forces account for at least 35% of the total adsorption energy, with such a contribution becoming stronger with respect to the size of the NC (up to 39% of the total adsorption energy with Pt_{20}). These results suggest that smaller Pt clusters might provide a more stable sensing platform with respect to larger nanoparticles, as the interaction between Pt and MoS_2 appears to grow weaker with the size of the metal cluster. Although we cannot certainly claim this to be a trend given the small number of Pt clusters considered in this work, we point out that similar results highlighting the impact of the size of Pt clusters on the adsorption energies were also found in systems with graphene as the support.[70–72]

The strong interaction between Pt NCs and MoS_2 is expected to lead to some charge transfer. Therefore, we computed net atomic charges with the DDEC method, and we found that, for each of the systems here considered, Pt clusters always act as the electron-donating species. Quantitatively, we found a non-negligible net charge transfer (ΔQ) of 0.31 $|e|$, 0.33 $|e|$, 0.39 $|e|$, and 0.43 $|e|$ for Pt_9, Pt_{13}, Pt_{16}, and Pt_{20}, respectively. Here, the size effect is evident, with the total amount of negative charge transferred from Pt clusters to the MoS_2 support steadily increasing with respect to the dimension of the NCs. It is worth noting that in our previous work, we found the amount of charge transfer from cortisol to bare MoS_2 to be only a small fraction of such values.[53]

To better understand the impact of the presence of Pt clusters on the electronic properties of MoS_2, we also computed the density of states (DOS) of each of the four MoS_2/Pt_n systems. We projected this quantity on MoS_2 only, and we compared it against the DOS of pristine single-layer MoS_2, as shown in Figure 4. From the DOS, it is evident that Pt clusters induce n-type doping on MoS_2, as the Fermi level of the material gets shifted closer to its conduction band. This correlates with the extra negative charge present on the surface of MoS_2 due to the presence of Pt clusters. Aside from such a doping effect, we note that the shape of the DOS is not significantly affected, indicating that MoS_2 still maintains its intrinsic properties. However, we could observe the presence of weak mid-gap states which become more delocalized and spread throughout the material's band gap with the increase of the clusters size. This suggests the weak metallization of MoS_2, at least with the larger Pt clusters.

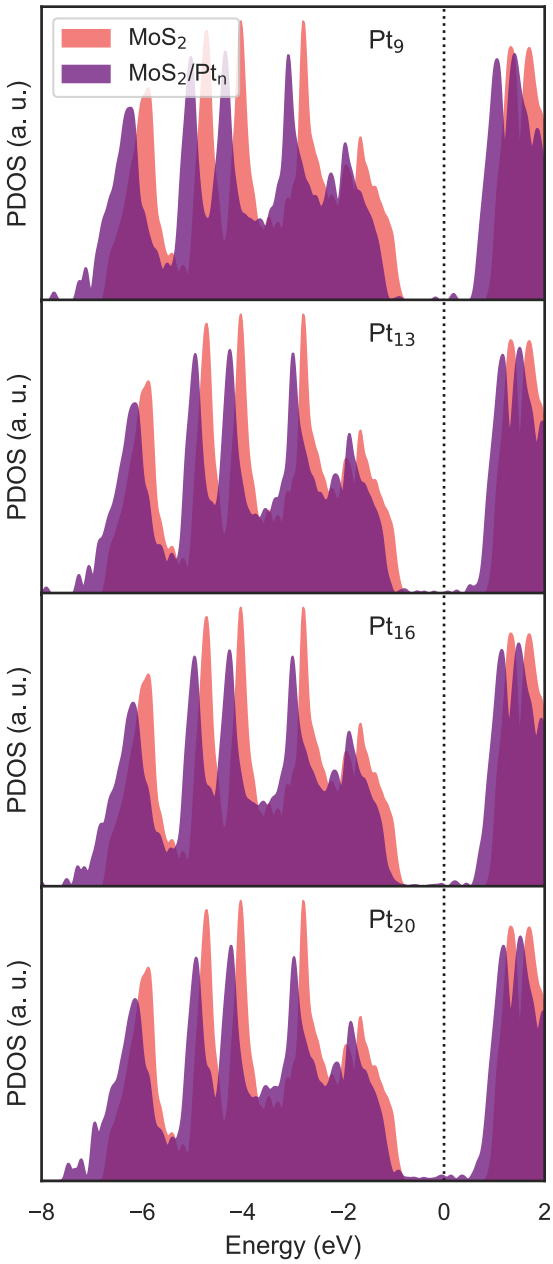

Figure 4: Density of states (PDOS) of the four MoS_2/Pt_n systems, projected on MoS_2 only and compared against the pristine material. The plots are centered around the Fermi level of the systems, and were obtained with a Gaussian smearing of 0.05 eV.

Table 1: Adsorption energies (in eV) computed via DFT of cortisol on the different adsorption sites of the Pt clusters considered in this work. To compute adsorption energies, the presence of the MoS_2 support was taken into account. Values in parentheses refer to the dispersion contribution towards the total adsorption energies.

	E_{ads} (eV)			
Ads. site	Pt_9	Pt_{13}	Pt_{16}	Pt_{20}
Vertex (A)	-3.53 (-0.96)	-2.95 (-1.35)	-3.78 (-1.79)	-2.98 (-2.14)
Edge (B)	-	-3.07 (-1.59)	-3.43 (-1.65)	-3.63 (-2.10)
Vertex (C)	-	-	-2.89 (-1.00)	-3.00 (-1.31)
Center (D)	-	-	-	-2.66 (-1.42)

3.2 Adsorption Mechanism

Following the assessment of the MoS_2/Pt_n sensing platform, we now discuss the adsorption mechanism of cortisol on supported Pt NCs by investigating adsorption energies and structural changes in the analyte.

We first focused on finding the most energetically favorable adsorption conformation of cortisol on supported Pt_n. As mentioned in the previous section, we only considered the carbonyl group of cortisol attached to ring A and we tested different adsorption sites on the surface of the NCs (see Figure 2). For each site, we computed the corresponding adsorption energy, which can be found in Table 1. In addition, to better understand the nature of the analyte/substrate interaction, we were able to decompose the total adsorption energy into its dispersion and electrostatic contributions. From Table 1 it is possible to observe that E_{ads} ranges between roughly -2.7 and -3.8 eV, a range of values compatible with chemisorption. Indeed, it is evident that for each system there exists a non negligible attractive electrostatic contribution, as that given by dispersion forces is lower than the total E_{ads}. We also note that, on average, the attractive electrostatic contribution appears to become weaker with the increase of the size of the NC, suggesting that with larger NCs dispersion may eventually become the main driving force for adsorption. This could potentially be beneficial for the device reusability, as it might be easier to desorb the cortisol molecule from the nanoparticle to reset the device. Finally, from E_{ads} it is clear that cortisol binds more favorably to MoS_2/Pt_9 and MoS_2/Pt_{16} on the vertex site (A), whereas the edge site (B) is preferred with MoS_2/Pt_{13} and MoS_2/Pt_{20}. Therefore, from now on we will focus only on such systems, whose optimized geometries are shown in Figure 5.

From the structural point of view, our results show that cortisol interacts with each NC synergistically via both its C=O and C=C groups. As already discussed, the analysis of E_{ads} suggests chemisorption to occur, and therefore we would expect the structure of cortisol and/or that of the NCs to be significantly affected once the adsorption event takes place. Indeed, this appears to be the case, as we observed by thoroughly investigating the variation of bond lengths and the formation of chemical bonds in the systems (see Figure 6). As can be seen, the Pt-O bond length ranges between 2.06 and 2.31 Å, with the shorter bond occurring with Pt_9. Also, it is evident from the same figure that one single Pt atom strongly interacts with both C4 and C5 of cortisol: for each of the supported NCs, we found a non negligible displacement of

the Pt atom interacting with C=C of cortisol, as the atom moves towards the analyte molecule. The Pt-C bond length ranges between 2.13 and 2.30 Å. Interestingly, we also observed a significant weakening of both C=O and C=C bonds of cortisol upon chemisorption, whose computed values in the isolated molecule were 1.24 Å and 1.36 Å, respectively. Pt_9 is the cluster that causes the most significant increase in C=O bond length, which increases from 1.24 Å to 1.32 Å. This may explain the higher electrostatic attraction force computed for cortisol on Pt_9. Following, is Pt_{16} with a C=O bond length of 1.29 Å, and then are Pt_{13} and Pt_{20} in which the bond length was found to be 1.27 Å. A similar increase of the bond length was observed also for C=C, which varied from 1.36 Å to 1.43-1.45 Å. On a final note, we point out that we did not observe any significant variation of the average MoS_2/cluster distance upon adsorption of cortisol, suggesting the stability of the MoS_2/Pt_n sensing substrate.

Overall, given the magnitude of E_{ads} and the non negligible change in bond lengths, we would expect a significant charge redistribution to occur upon cortisol adsorption.

3.3 Charge Transfer and Charge Redistribution

In this part, we focus on the electronic and charge-transfer effects in cortisol interacting with the MoS_2/Pt_n substrate.

We computed net atomic charges (ΔQ) by means of the DDEC6 method, and to spatially visualize the charge redistribution, we also computed the electron density difference (EDD) map for each of the four systems here considered. We found that the substrate acts as the charge acceptor, as in each case we obtained a positive net charge on the cortisol molecule, as can be seen in Table 3. From a quantitative point of view, we observed the net amount of charge transferred to increase with respect to the size of the NC, as the net positive charge on cortisol (ΔQ_{cor}) increases from +0.14 e with Pt_9 up to +0.22-0.24 e for larger NCs. Similarly, we observed the negative charge on MoS_2 (ΔQ_{MoS_2}) to increase, from -0.37 e per unit cell with Pt_9 up to -0.52 e with Pt_{20}.

By looking at the EDD maps in Figure 7, it is also possible to observe that charge redistribution occurs mainly in the proximity of the contact area between the ring A of cortisol and the Pt NC, with very little or no contribution coming from the analyte's backbone and tail. Moreover, we also note that the charge rearrangement appears to become more spatially localized with larger NCs, and this is particularly evident when comparing the EDD map of cortisol on Pt_9 against that of cortisol on Pt_{20}. Locally, the situation is more complex, as we found cortisol to possess both charge donating and attracting units. Thus, we selected few relevant atoms in the proximity of the bond between cortisol and Pt clusters, and we computed partial charges before (ΔQ_i) and after (ΔQ_f) adsorption. The results are shown in Table 2, from which it is possible to observe that O and C4 atoms both lose a significant amount of charge, and thus strongly contribute to the net charge loss of cortisol. On the other hand, C3 and C5 both gain some charge, and this is particularly evident in the case of Pt_9.

To sum up, our results suggest that, upon adsorption on Pt clusters, cortisol induces an extra amount of charge on MoS_2, whose magnitude increases with respect to the size of the cluster. This indicates that, if employing MoS_2 decorated with Pt NCs as the channel in FET sensors, larger nanoparticles may be beneficial in order to boost the response of the device. This occurs because such an extra charge induces an additional doping on the device channel, thus leading to a potentially measurable variation of the FET sensor characteristics. To assess the response of a model FET device, and to validate our proposed sensing mechanism, we then carried out device TCAD simulations.

Table 2: Net atomic charges of selected atoms of cortisol, computed by means of the DDEC6 method. ΔQ_i and ΔQ_f are the atomic charges before and after adsorption on the substrate, respectively.

Atom	ΔQ_i (e)	ΔQ_f (e)
	Pt_9	
O	−0.485	−0.347
C3	+0.439	+0.362
C4	−0.307	−0.245
C5	+0.136	+0.079
	Pt_{13}	
O	−0.485	−0.382
C3	+0.439	+0.427
C4	−0.307	−0.245
C5	+0.136	+0.097
	Pt_{16}	
O	−0.485	−0.345
C3	+0.439	+0.396
C4	−0.307	−0.237
C5	+0.136	+0.097
	Pt_{20}	
O	−0.485	−0.390
C3	+0.439	+0.416
C4	−0.307	−0.237
C5	+0.136	+0.100

Table 3: Net charge transfer (ΔQ) computed on each of the fragment of the investigated systems: MoS_2 (ΔQ_{MoS_2}), Pt NCs (ΔQ_{Pt}), and cortisol (ΔQ_{cor}).

System	ΔQ_{MoS_2} (e)	ΔQ_{Pt} (e)	ΔQ_{cor} (e)
Pt_9	-0.37	+0.23	+0.14
Pt_{13}	-0.41	+0.25	+0.16
Pt_{16}	-0.49	+0.25	+0.24
Pt_{20}	-0.52	+0.30	+0.22

3.4 Chemiresistive Response of MoS_2 FET Sensors

Here, we discuss our 2D TCAD simulations of electrical transport in MoS_2 back-gate FET to evaluate the range of possible responses of such devices to cortisol adsorption. As proof of concept, we consider only the two limiting cases: MoS_2 decorated with the smallest (Pt_9) and the largest (Pt_{20}) NCs. It is worth noting that, in both cases, we assumed the same cluster density of 1.8×10^{13} cm^{-2}, arising from our DFT simulations. The DFT-calculated charge transfer from Pt clusters to MoS_2 is emu-

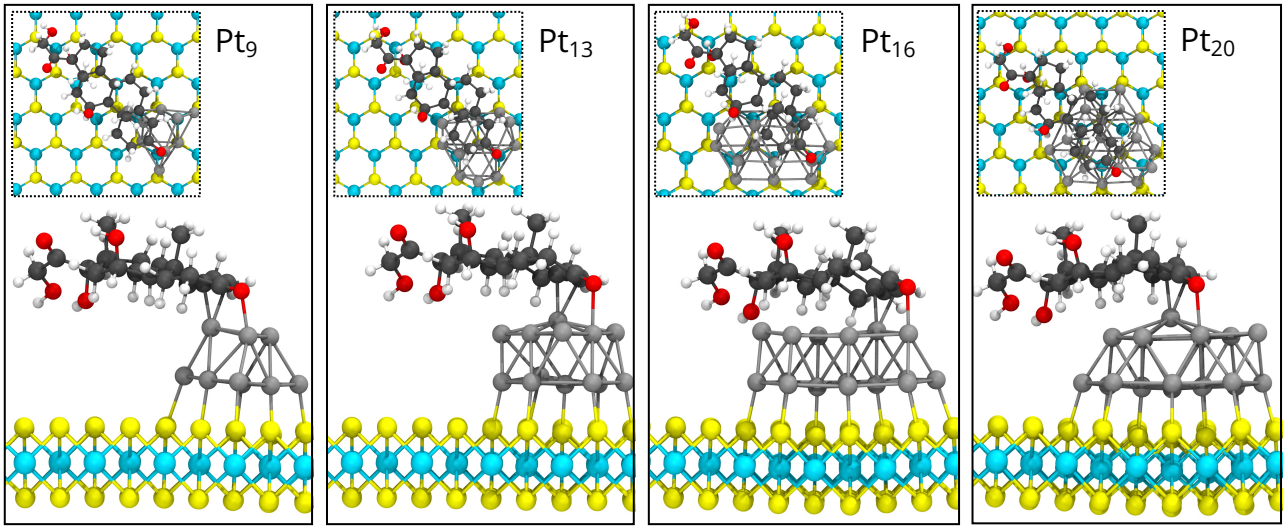

Figure 5: Optimized structures at the PBE-D2 level of cortisol on top of each of the four Pt clusters considered in this work. Here, only the four selected most energetically favored systems are shown.

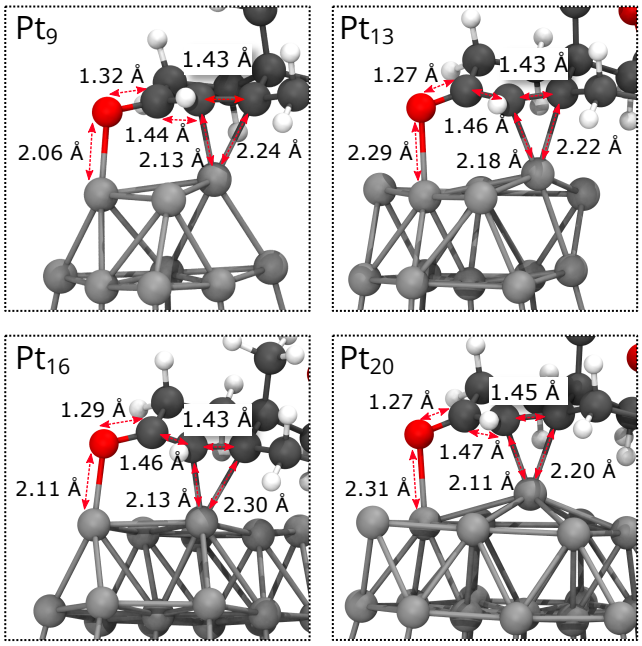

Figure 6: Bond lengths of cortisol in the proximity of the adsorption site with the Pt NCs.

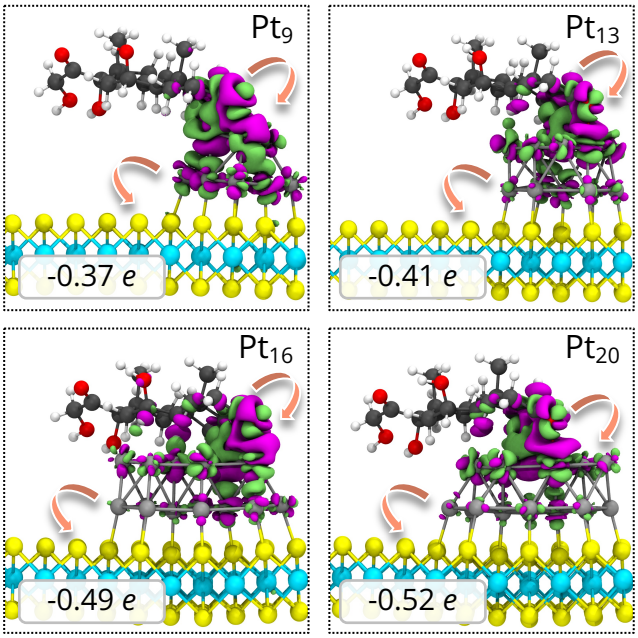

Figure 7: Electron density difference (EDD) maps of cortisol adsorbed on MoS_2/Pt_n. The color magenta corresponds to electron depletion, whereas color green to electron enrichment; isovalue 0.002 eV/Å^3. The total net computed charge on MoS_2 is also shown.

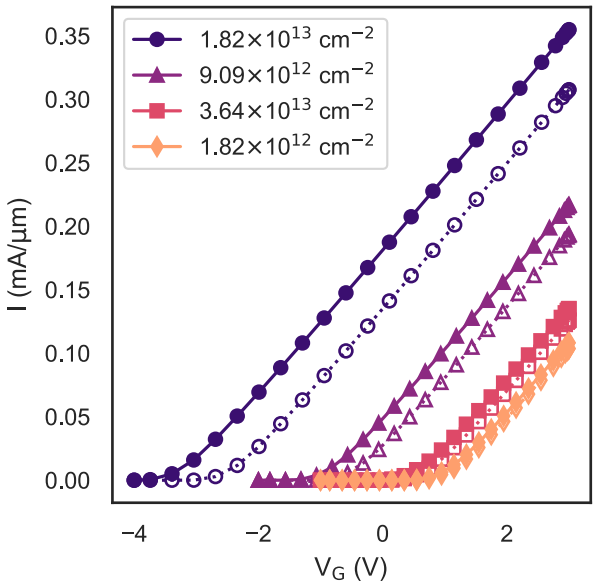

Figure 8: Simulated response characterisitcs of MoS_2 back-gate FET sensor device, whose channel is decorated with Pt_{20} clusters. The circle, triangle, square, and diamond markers correspond to decreasing Pt cluster densities of 1.82×10^{13}, 9.09×10^{12}, 3.64×10^{12} and 1.82×10^{12} cm^{-2}, respectively. Curves with empty markers represent the pristine device (i.e., with the MoS_2/Pt_{20} channel), whereas the curves with full markers represent the device with all the Pt NC sites occupied by cortisol molecules.

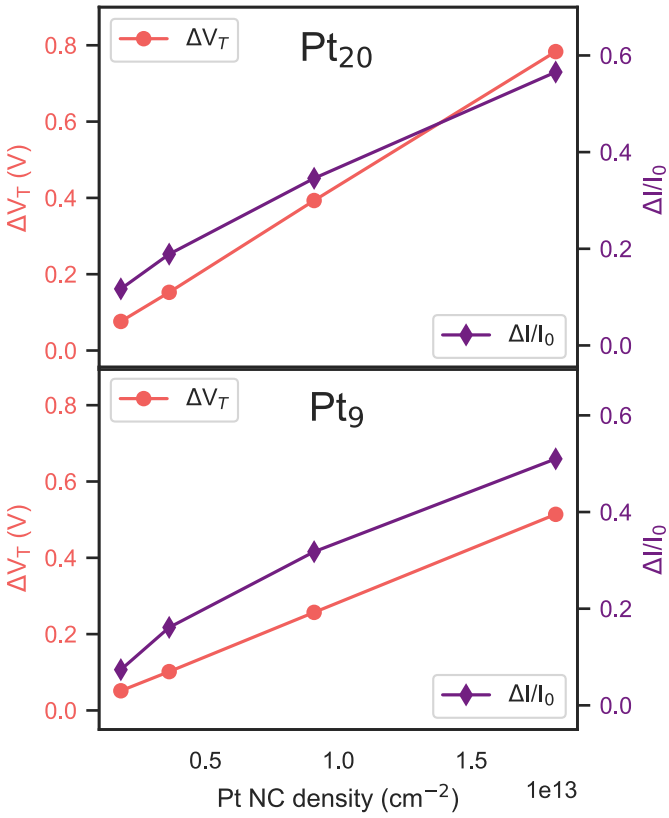

Figure 9: Typical metrics to assess the response of the simulated sensors to the analyte: the shift in threshold voltage (ΔV_T) and the normalized change in current ($\Delta I/I_0$). These are shown for the MoS_2 FET decorated with Pt_{20} (top plot), and Pt_9 (bottom plot). $\Delta I/I_0$ is calculated for values of current at V_G of -1.0 V and -0.3 V with Pt_{20} and Pt_9, respectively.

lated in TCAD simulations through n-type doping of the channel: 9.08×10^{19} cm^{-3} for Pt_9, and 1.26×10^{20} cm^{-3} for Pt_{20}. Similarly, the increase of charge trasfer induced by the adsoption of cortisol on the substrate is considered as n-doping of 1.08×10^{20} cm^{-3} for Pt_9, and of 1.52×10^{20} cm^{-3} for Pt_{20}. The reader is referred to Simulation Details for more information on how such doping values were obtained.

Figure 8 shows the simulated response characteristics of a FET device decorated with Pt_{20} clusters, before (empty markers) and after (full markers) cortisol adsorption. We point out that in the latter, a full occupancy of each Pt cluster by cortisol is assumed, due to the setup of DFT simulations. It can be observed that the analyte binding to the MoS_2 channel, mediated by the Pt NCs, produces a significant horizontal shift in the transfer characteristics of the devices as well as a vertical shift in current (ΔI) for any given value of gate voltage (V_G). Such a large threshold voltage shift (780 mV) can be easily measured experimentally, suggesting that the sensing approach proposed in this work could be very well suitable for detecting cortisol. However, we note that we are considering an ideal case in which the density of Pt NCs is rather high and with all the possible sites occupied. We expect a decrease of such a response with lower cluster densities. To assess this, we varied the density of the Pt clusters by rescaling the doping value obtained with DFT by a larger surface area. Here, we assumed that the amount of charge transferred from a single cortisol/Pt_n unit to MoS_2 remains constant when increasing the DFT simulation cell. This assumption is justified by having already simulated a large enough simulation cell, so that the interaction between periodic images of units of cortisol/Pt_n can be considered negligible (see Simulation Details). More specifically, we considered MoS_2 surface areas 2, 5, and 10 times larger, leading to NC densities of 9.09×10^{12} cm^{-2}, 3.64×10^{12} cm^{-2}, and 1.82×10^{12} cm^{-2}, respectively. Indeed, from Figure 8 we can observe the gate threshold voltage shift to decrease with respect to the NC density, up to 76 mV. We did not take into account lower NC densities, as this would lead to a gate threshold voltage shift below 76 mV. Such a low value would be of difficult detection under real device operation, due to intrinsic noise.

Figure 9 shows the variation of typical figures of merit[73] that we have extracted from our simulations: the shift in threshold voltage (ΔV_T) and the normalized change in current ($\Delta I/I_0$), set that I_0 is the initial current. Once again, we obtained such quantities from simulated curves at different cluster densities in MoS_2 decorated with Pt_{20} and Pt_9. As expected, ΔV_T is larger in MoS_2 decorated with the largest NCs, and this holds true for any cluster density here considered. However, $\Delta I/I_0$ is little affected by the size of the Pt cluster decorating the channel, and overall it ranges from $\sim$10% up to $\sim$50%.

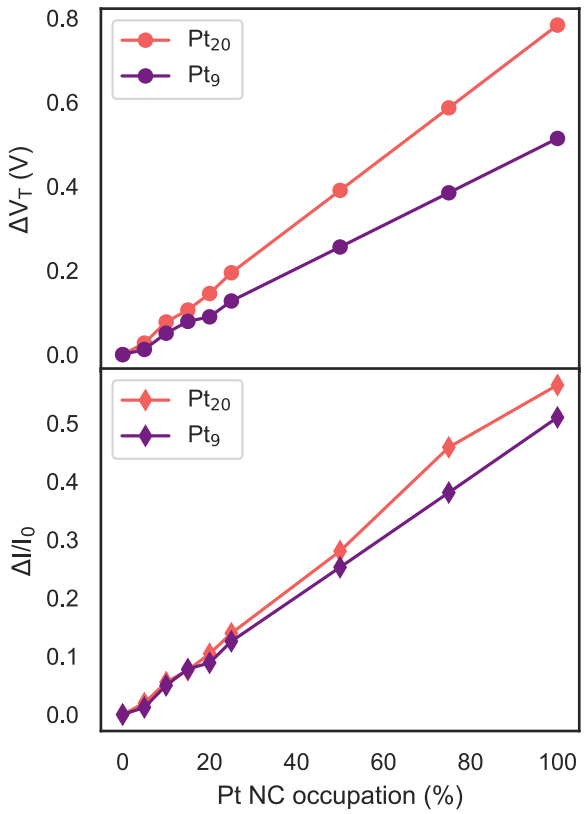

Figure 10: ΔV_T (top plot) and $\Delta I/I_0$ (bottom plot) against the percentage of NCs bound to cortisol, for devices decorated by both Pt_{20} and Pt_9. The TCAD simulations are performed considering the maximum NC density of 1.8×10^{13} cm^{-2}.

Finally, we considered the device with a cluster density of 1.8×10^{13} cm^{-2} (i.e., that resulting from our previous DFT simulations), and we simulated the variation of occupancy of Pt_{20} and Pt_9 NCs by cortisol molecules. To do so, we computed the difference between the net charge on the MoS_2 channel (which translates into doping) before and after the adsorption of cortisol (i.e., 0% and 100% occupancy, respectively): we assumed this value to be the maximum amount of extra charge (additional doping) due to the adsorption of cortisol. The equivalent doping densities due to partial occupancies were obtained by adding fractions of such an additional doping to the value of doping only due to the presence of Pt clusters. Results on sensors metrics are shown in Figure 10. One can observe that, with the Pt_{20}-decorated device, ΔV_T ranges from about 27 mV at 5% occupancy up to 780 mV at 100% occupancy, indicating that at smaller Pt NCs occupancies the device response may get lost in the noise. For the device decorated with Pt_9 clusters, we found ΔV_T to range from 12 mV at 5% occupancy up to 510 mV at 100% occupancy. Clearly, this is due to the limited amount of extra doping induced by the smaller clusters, further corroborating that larger Pt clusters might aid in the improvement of the device sensitivity. Correspondingly, we found the normalized change in current to vary, for both systems, from $\sim$2% up to $\sim$50%.

4 Conclusions

In conclusion, we were able to combine atomistic and device simulations with DFT and TCAD, which allowed us to successfully bridge the gap between materials properties and device physics. Our multi-scale simulation approach revealed that there exists a non-negligible chemical/physical interaction between cortisol and MoS_2 decorated with small sub-nanometer Pt clusters, thus making this material suitable as the channel in FET sensors.

4.1 Analyte and Sensing Material Interaction

At the materials' level, we found Pt clusters to strongly bind to the MoS_2 support, suggesting the stability of the sensing platform. In addition, we observed that decorating the 2D material with Pt clusters leads to the Pt-to-MoS_2 electron transfer, thus inducing n-type doping on MoS_2. We then explored the interaction between cortisol and supported Pt clusters, and we found that, from the structural point of view, the analyte binds to the NCs via both its carbonyl and C=C groups, causing a non-negligible decrease of both bond lengths. Also, our results suggest the occurring of chemisorption, which leads to the charge transfer from cortisol to the Pt clusters and the MoS_2 support. We were able to quantify the amount of charge transferred, and we used such values as starting point for our device simulations.

4.2 Proof-of-Concept Device Performance

At the device level, we simulated a FET sensor whose channel is MoS_2 decorated with Pt nanoclusters. By translating the net charge on MoS_2 before and after the adsorption of cortisol into additional n-type doping, we were able to assess and simulate

the device response. Indeed, we found that the presence of cortisol leads to a non-negligible shift of the FET threshold voltage, which could easily be measured. We assessed the performance of the device by extracting typical figures of merit, such as the variation of gate threshold voltage (ΔV_T) and the normalized change in current ($\Delta I/I_0$), with respect to: i) the density per unit area of Pt clusters and ii) the percentage of their occupancy by cortisol molecules. Our simulations showed that decreasing the NC density, as expected, leads to smaller values of ΔV_T to the point that the device sensitivity is limited by the unavoidable noise. This shows that the concentration of Pt clusters on MoS_2 needs to be carefully considered, in order to avoid any loss of sensitivity. Similarly, we found lower percentages of Pt NCs occupancies to also lead to a smaller device response.

4.3 Outlook and Challenges

Here, we stress that the simulations that we have carried out in this work are based on two main assumptions, among others: that there are no other interferents in the sample, and that cortisol only binds to Pt clusters and does not adsorb on MoS_2. Therefore, our results represent the maximum theoretical device response that can be achieved with this type of materials and architecture. Clearly, in a real device we expect such effects to significantly complicate both performance and response, as these are highly complex problems. Nevertheless, the first assumption is justified by the scope of our paper: to investigate the suitability of the chosen sensing platform (i.e., Pt nanoclusters deposited on single-layer MoS_2) towards the non-enzymatic detection of cortisol, as the development of non-enzymatic sensors is still a great challenge. Furthermore, cortisol binds more strongly to Pt clusters (chemisorption) rather than to MoS_2 (physisorption), and this justifies our second assumption. We hope our results can lay the necessary theoretical foundation for the development of novel point-of-care cortisol sensors based on metal-decorated 2D materials.

Acknowledgement

The authors ackowledge funding from the European Union's Horizon 2020 research and innovation programme, EU H2020 SmartVista project (www.smartvista.eu), grant agreement No. 825114. This work was granted access to the HPC/AI resources of IDRIS (Institut du Développement et des Ressources en Informatique Scientifique) under the allocation 2021-A0110811060 made by GENCI (Grand Équipement National de Calcul Intensif).

References

[1] J. Zhao, Y. Lin, J. Wu, H. Y. Y. Nyein, M. Bariya, L.-C. Tai, M. Chao, W. Ji, G. Zhang, Z. Fan, and A. Javey. A fully integrated and self-powered smartwatch for continuous sweat glucose monitoring. *ACS Sens.*, 4:1925–1933, 2019.

[2] Q. Cao, B. Liang, J. Mao, J. Wei, T. Tu, L. Fang, and X. Ye. A smartwatch integrated with a paper-based microfluidic patch for sweat electrolytes monitoring. *Electroanalysis*, 33:643–651, 2021.

[3] J. Kim, M. Kim, M.-S. Lee, K. Kim, S. Ji, Y.-T. Kim, J. Park, K. Na, K.-H. Bae, H. K. Kim, F. Bien, C. Y. Lee, and J.-U. Park. Wearable smart sensor systems integrated on soft contact lenses for wireless ocular diagnostics. *Nat. Commun.*, 8:14997, 2017.

[4] D. H. Keum, S.-K. Kim, J. Koo, G.-H. Lee, C. Jeon, J. W. Mok, B. H. Mun, K. J. Lee, E. Kamrani, C.-J. Joo, S. Shin, J.-Y. Sim, D. Myung, S. H. Yun, Z. Bao, and S. K. Hahn. Wireless smart contact lens for diabetic diagnosis and therapy. *Sci. Adv.*, 6:eaba3252, 2020.

[5] R. Gogurla, Y. Kim, S. Cho, J. Kim, and S. Kim. Multifunctional and ultrathin electronic tattoo for on-skin diagnostic and therapeutic applications. *Adv. Mater.*, 33:2008308, 2021.

[6] A. J. Bandodkar, W. Jia, and J. Wang. Tattoo-based wearable electrochemical devices: A review. *Electroanalysis*, 27:562–572, 2015.

[7] J. Kim, A. S. Campbell, B. Esteban-Fernández de Ávila, and J. Wang. Wearable biosensors for healthcare monitoring. *Nat. Biotechnol.*, 37:389–406, 2019.

[8] C. A. da Costa, C. F. Pasluosta, B. Eskofier, D. Bandeira da Silva, and C. da Rosa Righi. Internet of health things: Toward intelligent vital signs monitoring in hospital wards. *Artif. Intell. Med.*, 89:61–69, 2018.

[9] D. S. Celermajer, C. K. Chow, E. Marijon, N. M. Anstey, and K. S. Woo. Cardiovascular disease in the developing world: Prevalences, patterns, and the potential of early disease detection. *J. Am. Coll. Cardiol.*, 60:1207–1216, 2012.

[10] J. N. Cohn, L. Hoke, W. Whitwam, P. A. Sommers, A. L. Taylor, D. Duprez, R. Roessler, and N. Florea. Screening for early detection of cardiovascular disease in asymptomatic individuals. *Am. Heart J.*, 146:679–685, 2003.

[11] Theo Vos, Stephen S Lim, Cristiana Abbafati, Kaja M Abbas, Mohammad Abbasi, Mitra Abbasifard, Mohsen Abbasi-Kangevari, Hedayat Abbastabar, Foad Abd-Allah, Ahmed Abdelalim, et al. Global burden of 369 diseases and injuries in 204 countries and territories, 1990–2019: A systematic analysis for the global burden of disease study 2019. *The Lancet*, 396:1204–1222, 2020.

[12] Cardiovscular Diseases Fact Sheet, World Health Organization (WHO) (https://www.who.int/en/news-room/fact-sheets/detail/cardiovascular-diseases-(cvds)), Last accessed: Sep 19 2022.

[13] R. S. Vasan, M. G. Larson, E. P. Leip, J. C. Evans, C. J. O'Donnell, W. B. Kannel, and D. Levy. Impact of high-normal blood pressure on the risk of cardiovascular disease. *N. Engl. J. Med.*, 345:1291–1297, 2001.

[14] S. L. Stevens, S. Wood, C. Koshiaris, K. Law, P. Glasziou, R. J. Stevens, and R. J. McManus. Blood pressure variability and cardiovascular disease: Systematic review and meta-analysis. *BMJ*, 354:i4098, 2016.

[15] E. Iob and A. Steptoe. Cardiovascular disease and hair cortisol: a novel biomarker of chronic stress. *Curr. Cardiol. Rep.*, 21:116, 2019.

[16] J. A. Whitworth, P. M. Williamson, G. Mangos, and J. J. Kelly. Cardiovascular consequences of cortisol excess. *Vasc. Health Risk Manag.*, 1:291–299, 2005.

[17] Richard C. Stevens, Scott D. Soelberg, Steve Near, and Clement E. Furlong. Detection of cortisol in saliva with a flow-filtered, portable surface plasmon resonance biosensor system. *Anal. Chem.*, 80:6747–6751, 2008.

[18] Rosalba Gatti, Giorgia Antonelli, Maddalena Prearo, Paolo Spinella, Enrico Cappellin, and Elio F. De Palo. Cortisol assays and diagnostic laboratory procedures in human biological fluids. *Clin. Biochem.*, 42:1205–1217, 2009.

[19] Onur Parlak. Portable and wearable real-time stress monitoring: A critical review. *Sensors and Actuators Reports*, 3:100036, 2021.

[20] H. Park, S. Baek, A. Sen, B. Jung, J. Shim, Y. C. Park, L/ P/ Lee, Y. J. Kim, and S. Kim. Ultrasensitive and selective field-effect transistor-based biosensor created by rings of MoS_2 nanopores. *ACS Nano*, 16:1826–1835, 2022.

[21] M. Pali, B. Jagannath, K.-C. Lin, S. Upasham, D. Sankhalab, S. Upashama, S. Muthukumar, and S. Prasad. Catch (cortisol apta watch): 'bio-mimic alarm' to track anxiety, stress, immunity in human sweat. *Electrochim. Acta*, 390:138834, 2021.

[22] H.-B. Lee, M. Meeseepong, T. Q. Trung, B.-Y. Kim, and N.-E. Lee. A wearable lab-on-a-patch platform with stretchable nanostructured biosensor for non-invasive immunodetection of biomarker in sweat. *Biosens. Bioelectron.*, 156:112133, 2020.

[23] S. Klinghammer, T. Voitsekhivska, N. Licciardello, K. Kim, C.-K. Baek, H. Cho, K.-J. Wolter, C. Kirschbaum, L. Baraban, and G. Cuniberti. Nanosensor-based real-time monitoring of stress biomarkers in human saliva using a portable measurement system. *ACS Sens.*, 5:4081–4091, 2020.

[24] O. Parlak, S. T. Keene, A. Marais, V. F. Curto, and A. Salleo. Molecularly selective nanoporous membrane-based wearable organic electrochemical device for noninvasive cortisol sensing. *Sci. Adv.*, 4:eaar2904, 2018.

[25] H.-J. Jang, T. Lee, J. Song, L. Russell, H. Li, J. Dailey, P. C. Searson, and H. E. Katz. Electronic cortisol detection using an antibody-embedded polymer coupled to a field-effect transistor. *ACS Appl. Mater. Interfaces*, 10:16233–16237, 2018.

[26] Yo-Han Kim, Kyungmin Lee, Hunsang Jung, Hee Kyung Kang, Jihoon Jo, In-Kyu Park, and Hyun Ho Lee. Direct immune-detection of cortisol by chemiresistor graphene oxide sensor. *Biosens. Bioelectron.*, 98:473–477, 2017.

[27] Haider Ali, Ashish Yadav, and Nishith Verma. Facile measurement of cortisol using microchannel embedded cu-rgo-polymer composite chemiresistive sensor. *Chem. Eng. Process.*, 180:108656, 2022.

[28] Mohd Maidin Nur Nasyifa, A. Rahim Ruslinda, Nur Hamidah Abdul Halim, Azrul Syafiq Zainol Abidin, Fatin Nabilah Mohd Faudzi, Nurul Atiqah Ahmad, Zainovia Lockman, Bohuslav Rezek, Alexander Kromka, and Subash C.B. Gopinath. Immuno-probed graphene nanoplatelets on electrolyte-gated field-effect transistor for stable cortisol quantification in serum. *J. Taiwan Inst. Chem. Eng.*, 117:10–18, 2020.

[29] Deji Akinwande, Christopher J. Brennan, J. Scott Bunch, Philip Egberts, Jonathan R. Felts, Huajian Gao, Rui Huang, Joon-Seok Kim, Teng Li, Yao Li, Kenneth M. Liechti, Nanshu Lu, Harold S. Park, Evan J. Reed, Peng Wang, Boris I. Yakobson, Teng Zhang, Yong-Wei Zhang, Yao Zhou, and Yong Zhu. A review on mechanics and mechanical properties of 2d materials—graphene and beyond. *Extreme Mech. Lett.*, 13:42–77, 2017.

[30] R. Mas-Ballesté, C. Gómez-Navarro, J. Gómez-Herrero, and F. Zamora. 2d materials: to graphene and beyond. *Nanoscale*, 3:20–30, 2011.

[31] T. Li and G. Galli. Electronic properties of MoS_2 nanoparticles. *J. Phys. Chem. C*, 111:16192–16196, 2007.

[32] B. W. H. Baugher, H. O. H. Churchill, Y. Yang, and P. Jarillo-Herrero. Intrinsic electronic transport properties of high-quality monolayer and bilayer MoS_2. *Nano Lett.*, 13:4212–4216, 2013.

[33] H. Schmidt, S. Wang, L. Chu, M. Toh, R. Kumar, W. Zhao, A. H. Castro Neto, K. Martin, S. Adam, B. Özyilmaz, and G. Eda. Transport properties of monolayer MoS_2 grown by chemical vapor deposition. *Nano Lett.*, 14:1909–1913, 2014.

[34] Z. Yu, Z.-Y. Ong, Li S., J.-B. X, G. Zhang, Y.-W. Zhang, Y. Shi, and X. Wang. Analyzing the carrier mobility in transition-metal dichalcogenide MoS_2 field-effect transistors. *Adv. Funct. Mater.*, 17:1604093, 2017.

[35] D. Kinnamon, R. Ghanta, K.-C. Lin, S. Muthukumar, and S. Prasad. Portable biosensor for monitoring cortisol in low-volume perspired human sweat. *Sci. Rep.*, 7:13312, 2017.

[36] M. Sekar, M. Pandiaraj, S. Bhansali, N. Ponpandian, and C. Viswanathan. Carbon fiber based electrochemical sensor for sweat cortisol measurement. *Sci. Rep.*, 9:403, 2019.

[37] S. Dalirirad and A. J. Steckl. Aptamer-based lateral flow assay for point of care cortisol detection in sweat. *Sens. Actuators B Chem.*, 283:79–86, 2019.

[38] M. Mallesha, R. Manjunatha, G. S. Suresh, J. Savio Melo, S. F. D'Souza, and T. V. Venkatesha. Direct electrochemical non-enzymatic assay of glucose using functionalized graphene. *J. Solid State Electrochem.*, 16:2675–2681, 2020.

[39] Y. Xianyu, J. Sun, Y. Li, Y. Tian, Z. Wang, and X. Jiang. An ultrasensitive, non-enzymatic glucose assay via gold nanorod-assisted generation of silver nanoparticles. *Nanoscale*, 5:6303, 2013.

[40] R. Li, X. Deng, and L. Xia. Non-enzymatic sensor for determination of glucose based on ptni nanoparticles decorated graphene. *Sci. Rep.*, 10:16788, 2020.

[41] F. Mehmood and R. Patcher. Density functional theory study of chemical sensing on surfaces of single-layer MoS_2 and graphene. *J. Appl. Phys.*, 115:164302, 2014.

[42] Z. Zhang, K. Chen, Q. Zhao, M. Huang, and X. Ouyang. Effects of noble metal doping on hydrogen sensing performances of monolayer MoS_2. *Mater. Res. Express*, 7:015501, 2019.

[43] G. Cui, H. Zhang, X. Zhang, and J. Tang. Rh-doped $MoSe_2$ as a toxic gas scavenger: a first-principles study. *Nanoscale Adv.*, 1:772–780, 2019.

[44] J. Ortiz-Medina, F. López-Urías, H. Terrones, F. J. Rodríguez-Macías, M. Endo, and M. Terrones. Differential response of doped/defective graphene and dopamine to electric fields: A density functional theory study. *J. Phys. Chem. C*, 119:13972–13978, 2015.

[45] Y. Lei, D. Butler, M. C. Lucking, F. Zhang, T. Xia, K. Fujisawa, T. Granzier-Nakajima, R. Cruz-Silva, M. Endo, H. Terrones, M. Terrones, and A. Ebrahimi. Single-atom doping of MoS_2 with manganese enables ultrasensitive detection of dopamine: Experimental and computational approach. *Sci. Adv.*, 6:eabc4250, 2020.

[46] W. Van Roosbroeck. Theory of the flow of electrons and holes in germanium and other semiconductors. *Bell Syst. Tech. J.*, 29(4):560–607, 1950.

[47] Stefania Carapezzi, Sebastian Eberle, Susanna Reggiani, Elena Gnani, Cosmin Roman, Christofer Hierold, and Antonio Gnudi. 3d tcad modeling of no2cnt fet sensors. In *2018 48th European Solid-State Device Research Conference (ESSDERC)*, pages 222–225, 2018.

[48] S. Carapezzi, S. Reggiani, E. Gnani, and A. Gnudi. Tcad simulation framework of gas desorption in cnt fet NO_2 sensors. *IEEE Transactions on Electron Devices*, 67:4682–4686, 2020.

[49] Y. Shi, B. Song, R. Shahbazian-Yassar, J. Zhao, and W. A. Saidi. Experimentally validated structures of supported metal nanoclusters on MoS_2. *J. Phys. Chem. Lett.*, 9:2972–2978, 2018.

[50] R. E. Fernandez, Y. Umasankar, P. Manickam, Nickel J. C., L. R. Iwasaki, B. K. Kawamoto, K. C. Todoki, J. M. Scott, and S. Bhansali. Disposable aptamer-sensor aided by magnetic nanoparticle enrichment for detection of salivary cortisol variations in obstructive sleep apnea patients. *Sci. Rep.*, 7:17992, 2017.

[51] N. Suda, H. Sunayama, Y. Kitayama, Y. Kamon, and T. Takeuchi. Oriented, molecularly imprinted cavities with dual binding sites for highly sensitive and selective recognition of cortisol. *R. Soc. open sci.*, 4:170300, 2017.

[52] P. Manickam, R. E. Fernandez, Y. Umasankar, M. Gurusamy, F. Arizaleta, G. Urizar, and S. Bhansali. Salivary cortisol analysis using metalloporphyrins and multi-walled carbon nanotubes nanocomposite functionalized electrodes. *Sens. Actuators B Chem.*, 274:47–53, 2018.

[53] G. Boschetto and A. Todri-Sanial. Assessing doping strategies for monolayer MoS_2 towards non-enzymatic detection of cortisol: A first-principles study. *Phys. Chem. Chem. Phys.*, 24:1048–1058, 2022.

[54] S. F. Boys and F. Bernardi. The calculation of small molecular interactions by the differences of separate total energies. some procedures with reduced errors. *Mol. Phys.*, 19:553–566, 1970.

[55] S. Smidstrup, T. Markussen, P. Vancraeyveld, J. Wellendorff, J. Schneider, T. Gunst, B. Verstichel, D. Stradi, P. A. Khomyakov, U. G. Vej-Hansen, et al. Quantumatk: An integrated platform of electronic and atomic-scale modelling tools. *J. Phys: Condens. Matter*, 32:015901, 2020.

[56] QuantumATK version T-2022.03, Synopsys QuantumATK (www.synopsys.com/silicon/quantumatk.html).

[57] J. P. Perdew, K. Burke, and M. Ernzerhof. Generalized gradient approximation made simple. *Phys. Rev. Lett.*, 77:3865–3868, 1996.

[58] M. J. van Setten, M. Giantomassi, E. Bousquet, M. J. Verstraete, D. R. Hamann, X. Gonze, and G.-M. Rignanese. The pseudodojo: Training and grading a 85 element optimized norm-conserving pseudopotential table. *Comput. Phys. Commun.*, 226:39–54, 2018.

[59] Stefan Grimme. Semiempirical gga-type density functional constructed with a long-range dispersion correction. *J. Comput. Chem.*, 27(15):1787–1799, 2006.

[60] H. J. Monkhorst and J. D. Pack. Special points for brillouin-zone integrations. *Phys. Rev. B*, 13:5188–5192, 1976.

[61] T. A. Manz and N. Gabaldon Limas. Chargemol program for performing DDEC analysis, Version 3.5, 2017, (ddec.sourceforge.net).

[62] T. A. Manz and N. Gabaldon Limas. Introducing DDEC6 atomic population analysis: Part 1. charge partitioning theory and methodology. *RSC Adv.*, 6:47771–47801, 2016.

[63] T. A. Manz and N. Gabaldon Limas. Introducing [DDEC6 atomic population analysis: Part 2. computed results for a wide range of periodic and nonperiodic materials. *RSC Adv.*, 6:45727–45747, 2016.

[64] *Sentaurus Device User Guide, Version Q-2019.12*. Synopsys Inc., Mountain View, CA, USA, 2019.

[65] Theresia Knobloch, Gerhard Rzepa, Yury Yu. Illarionov, Michael Waltl, Franz Schanovsky, Bernhard Stampfer, Marco M. Furchi, Thomas Mueller, and Tibor Grasser. A physical model for the hysteresis in MoS_2 transistors. *IEEE J. Electron Devices Soc.*, 6:972–978, 2018.

[66] Bernhard Stampfer, Feng Zhang, Yury Yuryevich Illarionov, Theresia Knobloch, Peng Wu, Michael Waltl, Alexander Grill, Joerg Appenzeller, and Tibor Grasser. Characterization of single defects in ultrascaled MoS_2 field-effect transistors. *ACS Nano*, 12(6):5368–5375, 2018.

[67] Pin-Chun Shen, Cong Su, Yuxuan Lin, Ang-Sheng Chou, Chao-Ching Cheng, Ji-Hoon Park, Ming-Hui Chiu, Ang-Yu Lu, Hao-Ling Tang, Mohammad Mahdi Tavakoli, Gregory Pitner, Xiang Ji, Zhengyang Cai, Nannan Mao, Jiangtao Wang, Vincent Tung, Ju Li, Jeffrey Bokor, Alex Zettl, Chih-I Wu, Tomás Palacios, Li Lain-Jong, and Jing Kong. Ultralow contact resistance between semimetal and monolayer semiconductors. *Nature*, 593(7858):211–217, 2021.

[68] Ashima Rawat, Nityasagar Jena, Dimple, and Abir De Sarkar. A comprehensive study on carrier mobility and artificial photosynthetic properties in group vi b transition metal dichalcogenide monolayers. *J. Mater. Chem. A*, 6:8693–8704, 2018.

[69] Showkat Hassan Mir, Vivek Kumar Yadav, and Jayant Kumar Singh. Recent advances in the carrier mobility of two-dimensional materials: A theoretical perspective. *ACS Omega*, 5:14203–14211, 2020.

[70] W. B. Schneider, U. Benedikt, and A. A. Auer. Interaction of platinum nanoparticles with graphitic carbon structures: A computational study. *ChemPhysChem*, 14:2984–2989, 2013.

[71] S. Navalon, A. Dhakshinamoorthy, M. Alvaro, and H. Garcia. Metal nanoparticles supported on two-dimensional graphenes as heterogeneous catalysts. *Coord. Chem. Rev.*, 312:99–148, 2016.

[72] L. G. Verga, J. Aarons, M. Sarwar, D. Thompsett, A. E. Russell, and C.-K. Skylaris. Effect of graphene support on large pt nanoparticles. *Phys. Chem. Chem. Phys.*, 18:32713–32722, 2016.

[73] B. M. Lowe, K. Sun, I. Zeimpekis, C.-K. Skylaris, and N. G. Green. Field-effect sensors - from ph sensing to biosensing: Sensitivity enhancement using streptavidin-biotin as a model system. *Analyst*, 142:4173–4200, 2017.